

The Pulsating Eclipsing Binary TIC 309658221 in a 7.59 Day Orbit

Jae Woo Lee¹, Martti H. Kristiansen^{2,3}, and Kyeongsoo Hong⁴

¹*Korea Astronomy and Space Science Institute, Daejeon 34055, Korea*

²*DTU Space, National Space Institute, Technical University of Denmark, Elektrovej 327, DK-2800 Lyngby, Denmark*

³*Brorfelde Observatory, Observator Gyldenkernes Vej 7, DK-4340 Tølløse, Denmark*

⁴*Institute for Astrophysics, Chungbuk National University, Cheongju 28644, Korea*

jwlee@kasi.re.kr

ABSTRACT

We present a new eclipsing binary (EB) showing multiperiodic oscillations using the first three sectors of *TESS* photometry. The eclipse and pulsation light curves of TIC 309658221 were modeled using an iterative method to obtain a consistent photometric solution. The *TESS* target is a circular-orbit, detached binary system with a mass ratio of 0.349, an inclination angle of 80.42 deg, and a temperature difference of 847 K between the components. The primary component of the system lies near the red edge of the δ Sct instability region on the main-sequence band in the Hertzsprung-Russell diagram. Multiple frequency analyses were applied to the eclipse-subtracted residuals after removing the binary effects in the observed data. These resulted in the detection of 26 frequencies, of which $f_1 - f_6$ were independent pulsation frequencies. The 20 other frequencies could be mainly caused by orbital harmonics (f_8 and f_{11}) or combination frequencies. The period ratios and pulsation constants of the $f_1 - f_6$ frequencies are in the ranges of $P_{\text{pul}}/P_{\text{orb}} = 0.010 - 0.013$ and $Q = 0.027 - 0.036$ days, respectively, which are typical of δ Sct type. The results reveal that TIC 309658221 is an eclipsing δ Sct star with an orbital period of 7.5952 days and pulsation frequencies of 9.94–13.01 day⁻¹. This work demonstrates that the 2-min cadence observations of *TESS* are very useful for the study of pulsating EBs with multiple frequencies and low amplitudes.

Subject headings: asteroseismology — binaries: eclipsing — stars: fundamental parameters — stars: individual (TIC 309658221) — stars: oscillations (including pulsations)

1. INTRODUCTION

Near-continuous and ultra-precise photometric data have been obtained from space missions, such as *CoRoT* (Baglin et al. 2006; Auvergne et al. 2009) and *Kepler* (Borucki et al. 2010; Koch

et al. 2010). Although designed to search for extrasolar planets, these systems have revolutionized variable star studies, especially asteroseismology. The time-series data from these missions allow the detection of many pulsation frequencies with amplitudes lower than 0.1 mmag. Launched on 2018 April 18, the Transiting Exoplanet Survey Satellite (*TESS*) is a full-sky photometric survey to find small planets orbiting nearby stars 10–100 times brighter than those observed by *Kepler* (Ricker et al. 2015). It will survey over 85 % of the sky in a highly elliptical 13.7-day orbit during the 2-year primary mission. In this survey, each ecliptic hemisphere is divided into 13 partially overlapping sectors of $24 \text{ deg} \times 96 \text{ deg}$, each of which is continuously observed for two *TESS* orbits of 27.4 days. The satellite covers the southern ecliptic hemisphere in the first year and then observes the northern hemisphere in the following year.

EBs allow an accurate and direct determination of the masses and radii of stars, and pulsating stars allow stellar interiors to be probed from core to surface layers using asteroseismology. Then, the strong synergy between EBs and pulsators can play a critical reciprocal role in providing significant information on the stellar parameters and internal structures. We have been searching for and characterizing the pulsating EBs using *Kepler* photometry (Lee et al. 2014, 2019) and ground-based spectroscopy (Hong et al. 2015; Lee & Park 2018). In this paper, our program target is TIC 309658221 (HD 34954, TYC 8878-116-1, GSC 8878-0116, 2MASS J05170089-6130524; $V_T = +10.31$, $(B - V)_T = +0.35$; Høg et al. 2000), which was known as a single F-type star prior to the *TESS* observations (Stassun et al. 2018). Houk & Cowley (1975) classified the spectral type of the star as F2 III/IV but the classification might be deduced from the combined spectrum of the binary components. We show that this object is a new eclipsing binary with multiperiodic pulsations in a 7.59-day orbit.

2. *TESS* PHOTOMETRY AND ORBITAL PERIOD

The *TESS* with 2-s exposures provides 2-min cadence observations of more than 200,000 pre-selected stars and full-frame images of $24 \text{ deg} \times 96 \text{ deg}$ recorded every 30 min. TIC 309658221 was observed in a 2-min cadence mode from 2018 July 25. We used the simple aperture photometry data obtained during Sectors 1, 2, and 3 in camera 4 available at MAST¹. During our analysis, additional data for TIC 309658221 were released for Sections 4, 5 and 6 and we further note a continuous data stream in the southern hemisphere (Sector 1-13) using the Web *TESS* Viewing Tool². The uncorrected flux measurements were detrended and normalized following a procedure similar to that described by Lee et al. (2017). These were converted to a magnitude scale by applying a *TESS* magnitude of +9.84 (Stassun et al. 2018) at maximum light. We removed outliers that displayed quite a big deviation compared to neighboring observations by visual inspection, instead of automated sigma clipping because of the presence of the oscillation signal. As an example, the

¹<https://archive.stsci.edu/>

²<https://heasarc.gsfc.nasa.gov/cgi-bin/tess/webtess/wtv.py>

resultant light curve for Sector 1 is shown in Figure 1, where both eclipses and pulsations are clearly visible.

In order to obtain an orbital ephemeris for our program target, the times of minimum light and their errors were measured from the *TESS* observations by using the method of Kwee & van Woerden (1956). We applied a linear least-squares fit to the minimum times and determined the following ephemeris:

$$C_1 = \text{BJD } 2,458,365.204170(73) + 7.594648(23)E. \quad (1)$$

The parenthesized quantities are the 1σ uncertainty for the last digit of each term. Individual timing errors were used as weights. These are given in columns (1)–(5) of Table 1, where we present the $O-C_1$ values and epochs computed using equation (1). As shown in Figure 1 and discussed in the following sections, because TIC 30968221 is a pulsating EB exhibiting mutiperiodic oscillations, the eclipse times may be affected by the light variations. Hence, we recalculated the minimum times from each eclipse curve after subtracting all frequencies detected in Section 4 from the original *TESS* data. A linear fit to the new timings resulted in an improved ephemeris, as follows:

$$C_2 = \text{BJD } 2,458,365.206340(52) + 7.595165(17)E. \quad (2)$$

The results are presented in columns (6)–(8) of Table 1. The timing residuals of the ephemeris (2) show a standard deviation of ± 0.0024 d, which is over two times smaller than that (± 0.0064 d) of equation (1).

3. BINARY MODELING

A total of 52,776 individual observations from Sector 1 (BJD 2458325.29–2458353.17), Sector 2 (BJD 2458354.10–2458381.52), and Sector 3 (BJD 2458382.03–2458409.38) were modeled with the Wilson-Devinney synthesis code (Wilson & Devinney 1971, van Hamme & Wilson 2007; hereafter W-D). The effective temperature of the hotter primary star was set to be 6993 ± 200 K from Gaia DR2³ (Gaia Collaboration et al. 2018). We used the logarithmic limb-darkening coefficients taken from the tables of van Hamme (1993). Until now TIC 309658221 was known as a single star and no binary parameters exist. Thus, the binary modeling of the system was made in a way almost identical to that for the pulsating EBs KIC 11401845 (Lee et al. 2017) and EPIC 245932119 (Lee et al. 2019), applying the mass ratio (q)-search procedure to modes 2, 3, 4 and 5 of the W-D code. The differential correction (DC) program of the W-D code was carried out on each assumed mass ratio and the four modes, but only the light curve synthesis for detached mode 2 seemed to be acceptable for TIC 309658221, which had an optimal solution at $q = 0.35$.

From that time on, this value of q was treated as an adjustable parameter in deriving the light curve parameters of this binary. The DC program was run until the corrections to the parameters

³<https://gea.esac.esa.int/archive/>

became smaller than the corresponding standard deviations. The result is listed in Model 1 of Table 2. In order to estimate more reliable errors for the fitted parameters, the observed *TESS* data were divided into ten subsets and analyzed individually with the W-D code. Then, we computed the 1σ -values of each parameter from the ten different values (Koo et al. 2014). These values are given as parenthesized errors in Table 2. The synthetic light curve from Model 1 is given as a blue solid curve in the top panel of Figure 2 and the corresponding residuals are plotted in the middle panel of this figure. In all procedures including the q searches, we adjusted an orbital eccentricity (e) and a third light (l_3) as additional parameters, but their values remained indistinguishable from zero.

Assuming that the primary component is a normal main-sequence star, its surface temperature corresponds to a spectral type of $F1\pm 1$ and a mass of $M_1 = 1.50\pm 0.08 M_\odot$, based on their mutual relationship⁴ (Pecaut & Mamajek 2013). We computed the absolute dimensions for TIC 309658221 from the M_1 value and the light curve parameters in Table 2. These are presented in the lower part of Table 2. We calculated the absolute visual magnitudes (M_V) by using the bolometric corrections (BCs) of Torres (2010) between $\log T_{\text{eff}}$ and BC. The first distance to the EB system was determined to be 482 pc from an apparent magnitude of $V = +10.276$ (Høg et al. 2000) and the interstellar reddening of $A_V = 0.078$ (Schlafly & Finkbeiner 2011).

4. PULSATONAL CHARACTERISTICS

In Figure 3, the light curve residuals were plotted as the magnitudes *versus* BJDs. We could see oscillations with a semi-amplitude of about 6 mmag maximum and varying from cycle to cycle. To detect multiple frequencies in an iterative method (Lee et al. 2017, 2019), we applied frequency analyses to these residuals. The PERIOD04 program (Lenz & Breger 2005) was performed up to the Nyquist limit of $f_{\text{Ny}} = 360 \text{ day}^{-1}$. With the successive prewhitening process (Lee et al. 2014), we found the frequencies with the signal to noise amplitude ratio (S/N) larger than the empirical criterion of 4.0 proposed by Breger et al. (1993). Then, we analyzed the pulsation-subtracted data with the W-D code after removing the pulsation signatures from the original *TESS* data. New light curve parameters were used to obtain the corresponding eclipse-subtracted residuals, which were again introduced into the PERIOD04 program for multiple frequency analyses.

The above procedure was repeated until no significant signal was detected. The final light curve parameters and absolute dimensions are listed in Model 2 of Table 2, which are in good agreement with those from Model 1 within their errors. This indicates that the pulsations do not have much effect on the photometric solution of TIC 309658221. The pulsation-subtracted data and synthetic light curve are plotted as black circles and a red line, respectively, in the top panels of Figure 2. From the detailed analysis, we detected 26 frequencies with $S/N > 4.0$ listed in Table 3. The uncertainties for the frequency determination were calculated following the treatment of

⁴http://www.pas.rochester.edu/~emamajek/EEM_dwarf_UBVIJHK_colors_Teff.txt

Kallinger et al. (2008). The result from PERIOD04 is shown in Figure 4. The amplitude spectra after prewhitening the first six frequencies and then all 26 frequencies are presented in the second and bottom panels of Figure 4, respectively. The synthetic curve computed from the 26-frequency fit appears as a red line in the lower panel of Figure 3. We plotted the combination of the two effects (eclipses and pulsations) as green solid curves in Figure 1.

As shown in Figure 4 and Table 3, the main frequency peaks of TIC 309658221 lie in a region between 9 and 14 day⁻¹ and additional signals are visible at very low frequencies of < 1 day⁻¹. We examined the frequencies to identify possible harmonic and combination terms within the resolution of $1.5/\Delta t = 0.019$ day⁻¹, where $\Delta t = 81$ days is the time base of observations (Loumos & Deeming 1978). The result is presented in the last column of Table 3. The first six frequencies ($f_1 - f_6$) are pulsation frequencies, and the f_8 and f_{11} frequencies appear to be the orbital frequency of $f_{\text{orb}} = 0.13166$ day⁻¹ and its three times, respectively. The two low frequencies could be partially attributed to the imperfect removal of the binary effects in the *TESS* data. The majority of the remaining 18 frequencies mainly arise from combination frequencies.

5. SUMMARY AND DISCUSSION

TIC 309658221 was observed during Sectors 1, 2, and 3 of the *TESS* operations. The 2-min cadence observations exhibited both eclipses and oscillations, which implies that this object is not a single star but a pulsating EB. To improve binary and pulsation solutions, we analyzed the observed and prewhitened (eclipse- and pulsation-subtracted) data in an iterative process. The binary modeling indicates that TIC 309658221 is in a circular-orbit, detached configuration, where the primary and secondary components fill 27 % and 47 % of their inner Roche lobe, respectively. We estimated the absolute dimensions of each component from the photometric solutions and the empirical relations between effective temperature (spectral type) and stellar mass. As in previous studies (Lee et al. 2017; Lee & Park 2018), the binary parameters are immune to the oscillations. In mass-radius, mass-luminosity, and Hertzsprung-Russell (HR) diagrams (Lee et al. 2016; Lee & Park 2018), the primary component is a main-sequence star located near the red edge of the δ Sct instability strip. The low-mass secondary is highly oversized and overluminous, compared with dwarf stars of the same mass, but is not unusual for companions in short binaries (e.g., Table 1 of Liakos & Niarchos 2017).

We removed the binary effects in the observed *TESS* data and applied multiple frequency analyses to the light curve residuals. Twenty-six frequencies with S/N > 4.0 were detected in the two ranges of < 1 day⁻¹ and 8.0–20.5 day⁻¹. As shown in Table 3, $f_1 - f_6$ are independent pulsation frequencies, while the other frequencies may be orbital harmonics and combination terms. Using the Model 2 parameters in Table 2 and the equation of $\log Q_i = -\log f_i + 0.5 \log g + 0.1 M_{\text{bol}} + \log T_{\text{eff}} - 6.456$ (Petersen & Jørgensen 1972), we computed the observed pulsation constants of the six frequencies to be $Q_1 = 0.036$ days, $Q_2 = 0.034$ days, $Q_3 = 0.033$ days, $Q_4 = 0.027$ days, $Q_5 = 0.029$ days, and $Q_6 = 0.034$ days. The pulsation periods (P_{pul}) of 0.077–0.101 days and the

pulsation constants of 0.027–0.036 days correspond to pressure modes of δ Sct stars (Breger 2000). Further, $P_{\text{pul}}/P_{\text{orb}} = 0.010\text{--}0.013$ are within the upper limit of 0.09 for δ Sct pulsators in binaries (Zhang et al. 2013). These values and the position on the HR diagram reveal that the primary component of TIC 309658221 would be a δ Sct pulsator.

Our study demonstrates the potential of the 2-min cadence *TESS* data to characterize the pulsating stars in EBs. Despite our success in modeling TIC 309658221, the binary parameters are preliminary because of the absence of spectroscopic data. The pulsating EB is a relatively bright star with a long orbital period, so it is possible to carry out spectroscopic follow-up observations with 2-m class telescopes and to measure double-lined radial velocities. When high-resolution spectroscopy is undertaken, the accurate absolute masses, radii, temperatures, and luminosities can be directly derived and, hence, the physical properties of the system will be understood better than is possible with photometry alone.

This paper includes data collected by the *TESS* mission, which are publicly available from MAST. Funding for the *TESS* mission is provided by the NASA Science Mission directorate. We acknowledge the use of public *TESS* Alert data from pipelines at the TESS Science Office and at the TESS Science Processing Operations Center. This research has made use of the Simbad database maintained at CDS, Strasbourg, France, and was supported by the KASI grant 2019-1-830-03. K.H. was supported by the grant numbers 2017R1A4A1015178 of the National Research Foundation (NRF) of Korea.

REFERENCES

- Auvergne, M., Bodin, P., Boissard, L., et al. 2009, *A&A*, 506, 411
- Baglin, A., Auvergne, M., Boissard, L., et al. 2006, in 36th COSPAR Scientific Assembly (Paris: COSPAR), 3749
- Borucki, W. J., Koch, D., Basri, G., et al. 2010, *Sci*, 327, 977
- Breger, M. 2000, in ASP Conf. Ser. 210, *Delta Scuti and Related Stars*, ed. M. Breger, & M. H. Montgomery (San Francisco: ASP), 3
- Breger, M., Stich, J., Garrido, R., et al. 1993, *A&A*, 271, 482
- Gaia Collaboration, Brown, A. G. A., Vallenari, A., et al. 2018, *A&A*, 616, A1
- Høg, E., Fabricius, C., Makarov, V. V., et al. 2000, *A&A*, 355, 27
- Hong, K., Lee, J. W., Kim, S.-L., et al. 2015, *AJ*, 150, 131
- Houk, N., & Cowley, A. P. 1975, *University of Michigan Catalogue of Two-dimensional Spectral Types for the HD Stars, Vol. 1* (Ann Arbor, MI: University of Michigan)
- Kallinger, T., Reegen, P., & Weiss, W. W. 2008, *A&A*, 481, 571
- Koch, D. G., Borucki, W. J., Basri, G., et al. 2010, *ApJ*, 713, L79
- Koo, J.-R., Lee, J. W., Lee, B.-C., et al. 2014, *AJ*, 147, 104
- Kwee, K. K., & van Woerden, H. 1956, *BAN*, 12, 327
- Lee, J. W., & Park, J.-H. 2018, *MNRAS*, 480, 4693
- Lee, J. W., Kim, S.-L., Hong, K., Lee, C.-U., & Koo, J.-R. 2014, *AJ*, 148, 37
- Lee, J. W., Hong, K., Kim, S.-L., & Koo, J.-R. 2016, *MNRAS*, 460, 4220
- Lee, J. W., Hong, K., Kim, S.-L., & Koo, J.-R. 2017, *ApJ*, 835, 189
- Lee, J. W., Hong, K., & Kristiansen, M. H. 2019, *AJ*, 157, 17
- Lenz, P., & Breger, M. 2005, *Comm. Asteroseismology*, 146, 53
- Liakos, A., & Niarchos, P. 2017, *MNRAS*, 465, 1181
- Loumos, G. L., & Deeming, T. J. 1978, *Ap&SS*, 56, 285
- Pecaut, M. J., & Mamajek, E. E. 2013, *ApJS*, 208, 9
- Petersen, J. O., & Jørgensen, H. E. 1972, *A&A*, 17, 367

Ricker, G. R., Winn, J. N., Vanderspek, R., et al. 2015, *JATIS*, 1, 014003

Schlafly, E. F., & Finkbeiner, D. P. 2011, *AJ*, 737, 103

Stassun, K. G., Oelkers, R. J., Pepper, J., et al. 2018, *AJ*, 156, 102

Torres, G. 2010, *AJ*, 140, 1158

Van Hamme, W. 1993, *AJ*, 106, 209

Van Hamme, W., & Wilson, R. E. 2007, *ApJ*, 661, 1129

Wilson, R. E., & Devinney, E. J. 1971, *ApJ*, 166, 605

Zhang, X. B., Luo, C. Q., & Fu, J. N. 2013, *ApJ*, 777, 77

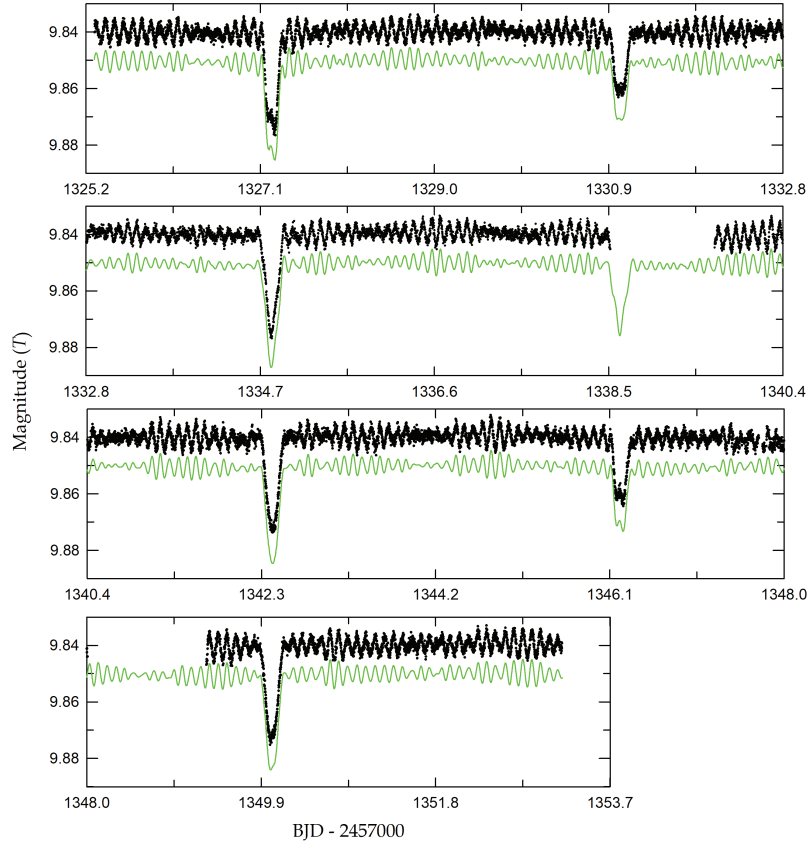


Fig. 1.— Black circles present time-series data of TIC 309658221 observed during the *TESS* Sector 1 and separated at intervals of 7.6 days. The green lines are the sum of the two model curves computed from the Model 2 parameters of Table 2 and the 26-frequency fit of Table 3, respectively. They are offset by +0.01 mag for clarity.

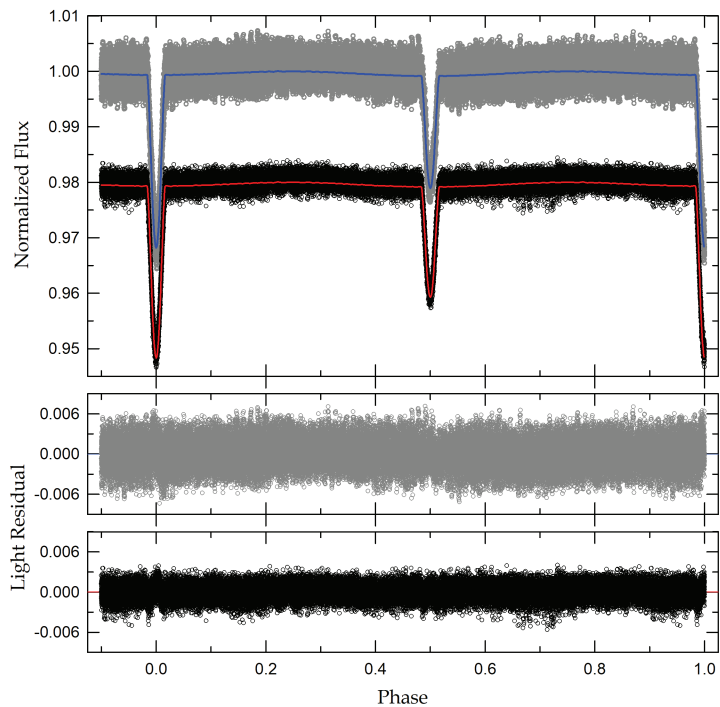


Fig. 2.— Binary light curve before (gray circle) and after (black circle) subtracting the pulsation signatures from the observed *TESS* data. The blue and red lines are computed with the Model 1 and Model 2 parameters of Table 1, respectively. The corresponding residuals from the fits are plotted in the middle and bottom panels in the same order as the light curves.

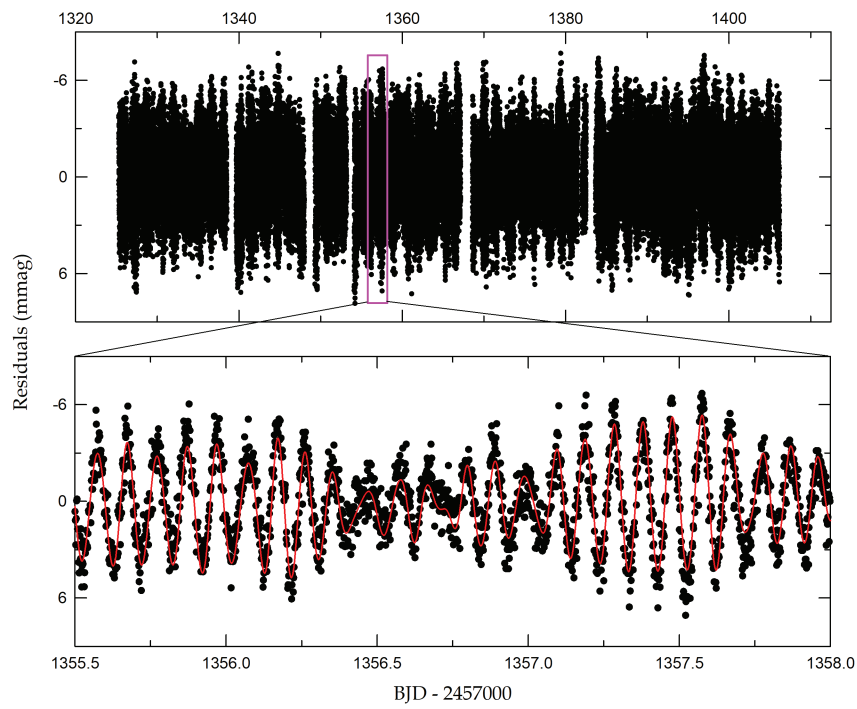


Fig. 3.— Light curve residuals after removing the binarity effect from the observed *TESS* data. The lower panel presents a short section of the residuals marked by the inset box in the upper panel. The synthetic curve is computed from the 26-frequency fit to the entire residuals.

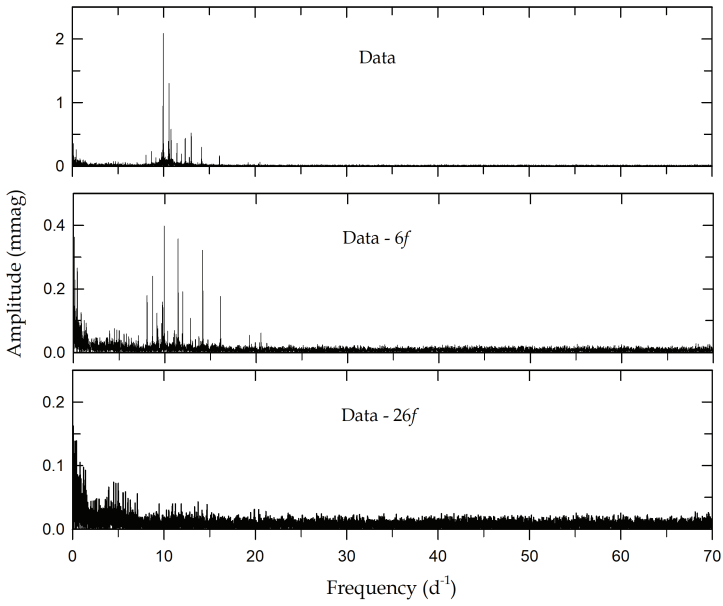


Fig. 4.— Amplitude spectra before (top panel) and after pre-whitening the first six frequencies (second) and all 26 frequencies (bottom) from the PERIOD04 program for all light residuals.

Table 1. Eclipse Timings Measured from Both Datasets: Including and Removing the Pulsation Signatures

Including Pulsations			Epoch	Min	Removing Pulsations		
BJD	Error	$O-C_1$			BJD	Error	$O-C_2$
2,458,327.22805	± 0.00048	-0.00289	-5.0	I	2,458,327.23049	± 0.00028	-0.00003
2,458,331.02846	± 0.00016	+0.00021	-4.5	II	2,458,331.02831	± 0.00016	-0.00021
2,458,334.82567	± 0.00054	+0.00009	-4.0	I	2,458,334.82586	± 0.00026	-0.00018
2,458,342.42052	± 0.00024	+0.00030	-3.0	I	2,458,342.42080	± 0.00021	-0.00004
2,458,346.21746	± 0.00074	-0.00009	-2.5	II	2,458,346.22076	± 0.00041	-0.00233
2,458,350.01585	± 0.00023	+0.00097	-2.0	I	2,458,350.01571	± 0.00020	-0.00030
2,458,357.61243	± 0.00137	+0.00291	-1.0	I	2,458,357.61032	± 0.00027	-0.00086
2,458,361.40918	± 0.00023	+0.00234	-0.5	II	2,458,361.40929	± 0.00022	-0.00053
2,458,365.20931	± 0.00087	+0.00514	+0.0	I	2,458,365.20614	± 0.00028	-0.00020
2,458,369.00414	± 0.00052	+0.00265	+0.5	II	2,458,369.00416	± 0.00021	-0.00023
2,458,372.80036	± 0.00063	+0.00154	+1.0	I	2,458,372.80056	± 0.00016	-0.00095
2,458,376.59548	± 0.00053	-0.00066	+1.5	II	2,458,376.59942	± 0.00023	-0.00033
2,458,380.39662	± 0.00027	+0.00315	+2.0	I	2,458,380.39645	± 0.00028	-0.00022
2,458,384.18102	± 0.00018	-0.00977	+2.5	II	2,458,384.19322	± 0.00043	-0.00103
2,458,387.99114	± 0.00043	+0.00302	+3.0	I	2,458,387.99117	± 0.00018	-0.00067
2,458,391.78882	± 0.00034	+0.00338	+3.5	II	2,458,391.78684	± 0.00024	-0.00258
2,458,395.60799	± 0.00059	+0.02523	+4.0	I	2,458,395.59629	± 0.00026	-0.00929
2,458,399.38446	± 0.00039	+0.00437	+4.5	II	2,458,399.38237	± 0.00027	-0.00221
2,458,403.18110	± 0.00036	+0.00369	+5.0	I	2,458,403.18140	± 0.00021	-0.00076

Table 2. Binary Parameters of TIC 309658221

Parameter	Model 1 ^a		Model 2 ^b	
	Primary	Secondary	Primary	Secondary
q	0.3494(43)		0.3491(17)	
i (deg)	80.463(82)		80.419(67)	
T (K)	6993(200)	6166(157)	6993(200)	6146(152)
Ω	9.448(91)	5.474(62)	9.428(72)	5.448(45)
Ω_{in}	2.573		2.573	
A	1.0	0.5	1.0	0.5
g	1.0	0.32	1.0	0.32
X, Y	0.639, 0.255	0.639, 0.230	0.639, 0.255	0.639, 0.230
x, y	0.615, 0.296	0.657, 0.277	0.615, 0.296	0.658, 0.277
$L/(L_1+L_2)$	0.7276(38)	0.2724	0.7288(15)	0.2712
r (pole)	0.1099(12)	0.0842(23)	0.1101(9)	0.0846(9)
r (point)	0.1101(12)	0.0845(23)	0.1103(9)	0.0849(9)
r (side)	0.1100(12)	0.0843(23)	0.1102(9)	0.0847(9)
r (back)	0.1101(12)	0.0845(23)	0.1103(9)	0.0849(9)
r (volume) ^c	0.1100(12)	0.0843(23)	0.1102(9)	0.0848(9)
$\sum W(O - C)^2$	0.0021		0.0011	
Absolute parameters:				
M (M_{\odot})	1.50(8)	0.52(3)	1.50(8)	0.52(3)
R (R_{\odot})	2.26(6)	1.73(6)	2.26(5)	1.74(4)
$\log g$ (cgs)	3.91(3)	3.68(4)	3.90(3)	3.67(3)
ρ (g cm ³)	0.18(2)	0.14(2)	0.18(2)	0.14(1)
L (L_{\odot})	11(1)	3.9(5)	11(1)	3.9(4)
M_{bol} (mag)	2.13(14)	3.26(13)	2.13(13)	3.26(12)
BC (mag)	0.03(1)	−0.02(2)	0.03(1)	−0.03(2)
M_V (mag)	2.10(14)	3.28(14)	2.10(13)	3.29(12)
Distance (pc)	482±31		482±30	

^aResult from the observed data.

^bResult from the pulsation-subtracted data.

^cMean volume radius.

Table 3. Multiple Frequency Analysis of TIC 309658221^a

	Frequency (day ⁻¹)	Amplitude (mmag)	Phase (rad)	S/N ^b	Remark
f_1	9.94597±0.00002	2.07±0.02	3.99±0.02	208.42	
f_2	10.57708±0.00003	1.31±0.02	0.98±0.04	128.87	
f_3	10.80865±0.00007	0.59±0.02	5.32±0.09	57.69	
f_4	13.00705±0.00008	0.53±0.02	2.71±0.09	52.82	
f_5	12.34430±0.00010	0.45±0.02	1.42±0.11	44.24	
f_6	10.50692±0.00010	0.44±0.02	0.91±0.11	43.93	
f_7	9.91961±0.00010	0.41±0.02	3.19±0.12	41.29	$f_2 + f_5 - f_4$
f_8	0.13278±0.00035	0.38±0.05	3.41±0.42	11.87	f_{orb}
f_9	11.44596±0.00012	0.36±0.02	1.87±0.14	35.50	$f_2 + f_3 - f_1$
f_{10}	14.14393±0.00012	0.32±0.02	0.92±0.15	33.88	$f_4 + 2f_6 - 2f_1$
f_{11}	0.41322±0.00045	0.30±0.05	4.64±0.54	9.26	$3f_{\text{orb}}$
f_{12}	8.66007±0.00018	0.24±0.02	5.70±0.22	23.18	$2f_6 - f_5$
f_{13}	11.95355±0.00022	0.19±0.02	1.20±0.27	18.77	$f_{10} + f_3 - f_4$
f_{14}	16.09894±0.00020	0.18±0.01	3.77±0.24	21.10	$2f_4 - f_7$
f_{15}	8.05874±0.00025	0.18±0.02	5.70±0.29	17.02	$f_{12} + f_7 - f_6$
f_{16}	9.73286±0.00025	0.16±0.02	5.17±0.30	16.55	$f_1 + f_2 - f_3$
f_{17}	9.14022±0.00035	0.12±0.02	1.71±0.42	12.02	$f_2 + f_6 - f_{13}$
f_{18}	12.79873±0.00040	0.11±0.02	4.09±0.48	10.51	$f_{13} + f_3 - f_1$
f_{19}	9.65329±0.00053	0.08±0.02	2.54±0.63	7.91	$f_1 + f_6 - f_3$
f_{20}	9.23767±0.00062	0.07±0.02	3.89±0.74	6.80	$f_{19} - f_{11}$
f_{21}	9.93635±0.00375	0.01±0.02	0.67±4.46	1.12	f_1
f_{22}	20.52151±0.00059	0.06±0.01	5.10±0.70	7.14	$f_1 + f_2$
f_{23}	10.30834±0.00070	0.06±0.02	1.99±0.83	6.03	$f_2 - 2f_{\text{orb}}$
f_{24}	11.04152±0.00072	0.06±0.02	4.55±0.86	5.86	$f_9 - f_{11}$
f_{25}	19.23727±0.00065	0.05±0.01	6.17±0.77	6.50	$f_{12} + f_2$
f_{26}	13.72771±0.00095	0.04±0.02	3.93±1.13	4.42	$f_{10} - f_{11}$

^aFrequencies are listed in order of detection.

^bCalculated in a range of 5 day⁻¹ around each frequency.